

Monte Carlo calculation of nine megavoltage photon beam spectra using the BEAM code

Daryoush Sheikh-Bagheri^{a)} and D. W. O. Rogers^{b)}

Ionizing Radiation Standards, National Research Council of Canada Ottawa, Ontario, K1A 0R6, Canada

(Received 10 August 2001; accepted for publication 13 November 2001; published 21 February 2002)

A recent paper analyzed the sensitivity to various simulation parameters of the Monte Carlo simulations of nine beams from three major manufacturers of commercial medical linear accelerators, ranging in energy from 4–25 MV. In this work the nine models are used: to calculate photon energy spectra and average energy distributions and compare them to those published by Mohan *et al.* [Med. Phys. **12**, 592–597 (1985)]; to separate the spectra into primary and scatter components from the primary collimator, the flattening filter and the adjustable collimators; and to calculate the contaminant-electron fluence spectra and the electron contribution to the depth-dose curves. Notwithstanding the better precision of the calculated spectra, they are similar to those calculated by Mohan *et al.* The three photon spectra at 6 MV from the machines of three different manufacturers show differences in their shapes as well as in the efficiency of bremsstrahlung production in the corresponding target and filter combinations. The contribution of direct photons to the photon energy fluence in a 10×10 field varies between 92% and 97%, where the primary collimator contributes between 0.6% and 3.4% and the flattening filter contributes between 0.6% and 4.5% to the head-scatter energy fluence. The fluence of the contaminant electrons at 100 cm varies between 5×10^{-9} and 2.4×10^{-7} cm⁻² per incident electron on target, and the corresponding spectrum for each beam is relatively invariant inside a 10×10 cm² field. On the surface the dose from electron contamination varies between 5.7% and 11% of maximum dose and, at the depth of maximum dose, between 0.16% and 2.5% of maximum dose. The photon component of the percentage depth-dose at 10 cm depth is compared with the general formula provided by AAPM's task group 51 and confirms the claimed accuracy of 2%. © 2002 American Association of Physicists in Medicine. [DOI: 10.1118/1.1445413]

Key words: Monte Carlo, photon spectra, electron contamination, head-scatter, mega-voltage photon beams

I. INTRODUCTION

In a companion paper¹ (which we will refer to as paper I) we have discussed a method to obtain parameters of the electron beam incident on the target of megavoltage photon beams by matching simulations to measurements. In this paper we discuss the results of those simulations in terms of depth-dose characteristics and photon and electron spectra for nine beams. Megavoltage photon beam spectra or various quantities based on them are used in many advanced treatment planning systems. There have been various experimental methods used to derive such spectra.^{2–19} However, the Monte Carlo method remains the most comprehensive and potentially the most accurate method of obtaining such spectra. Almost two decades ago, Mohan *et al.*²⁰ provided a series of megavoltage photon beam spectra for various energies of the Varian linacs using the Monte Carlo technique. Using simplified models they simulated only Varian machines, without deriving any of the incident electron beam parameters. Due to the limited computing power available at the time their spectra suffered from statistical noise. There have been a large number of papers since then in which Monte Carlo techniques have been used to calculate accelerator spectra and in paper I we have cited 20 such papers. Calculating such spectra with more accuracy requires knowledge of the characteristics of the electron beam incident on the

target as well as better tools for modelling the linac. In paper I we used the BEAM code system²¹ and derived best estimates for the mean energy and radial intensity distributions of the electron beam incident on the target. This was done by comparing calculated and measured values of in-air off-axis factors for large fields, together with calculated and measured central-axis relative depth-dose curves. The off-axis factor is measured in air and is the ratio of dose (taken as a ratio of ion chamber readings with a full buildup cap or miniphantom) at an off-axis point to the dose on the central axis at a given SSD, usually at 100 cm. In paper I, we also used off-axis factors to study the sensitivity of our linac models to various parameters, including, but not limited to, variations in the energy spectrum and intensity distribution of the incident electron beam, and the specifications of the primary collimator and the flattening filter. In this paper we present the photon spectra generated by the benchmarked accelerators, obtained in paper I, and compare them to the previously published spectra of Mohan *et al.*²⁰ The beams studied range from 4 MV to 25 MV in nominal energy and represent linacs made by the three major manufacturers. We highlight variations between different machines of quantities such as fractions of scatter from various components and electron contamination.

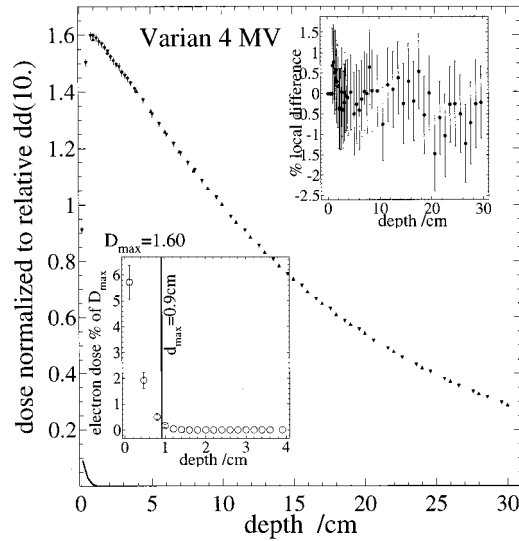


FIG. 1. Comparison of the calculated (using a 0.15 cm FWHM, 3.7 MeV electron beam with 3% FWHM energy spread) (\blacktriangledown) and the measured (\blacktriangle) central-axis depth-dose data for the 4 MV photon beam of the Varian low-energy accelerator (10×10 cm² field at 100 cm SSD). The upper-right inset shows the local difference (calc-meas) between the calculations and measurements in percent. Where no measured data are available, the difference is assigned a value of zero with no error bars. The lower-left inset shows the electron contamination (also shown as the solid line in the main panel) around depth of maximum dose (shown by the vertical line).

II. CENTRAL-AXIS DEPTH-DOSE CHARACTERISTICS

A. Total Dose

Figures 1–9 show the comparison between the calculated depth-dose distributions and the measurements for all the beams studied in this work. All measurements (depth dose

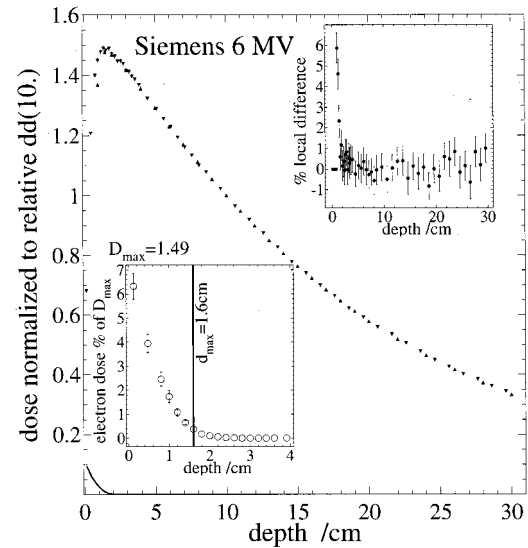


FIG. 3. Comparison of the calculated (using a 0.32 cm FWHM, 6.8 MeV electron beam with 14% FWHM energy spread) (\blacktriangledown) and the measured (\blacktriangle) central-axis depth-dose data for the 6 MV photon beam of the Siemens KD accelerator. Otherwise as in Fig. 1.

and off-axis factors) are from the compilation of task group 46 of the American Association of Physicists in Medicine (TG-46),²² unless specified otherwise in the captions of Figs. 1–9. When comparing the simulations with the measurements all data are normalized to the value of dose at 10 cm depth [$dd(10)$], which is obtained from a fourth order polynomial fit to the fall-off region of the depth-dose curve on the central axis (from 2 cm past depth of maximum dose to a depth of about 21 cm). To provide a more sensitive comparison of calculated and measured depth-dose values, difference plots are shown in the insets in Figs. 1–9. The insets show

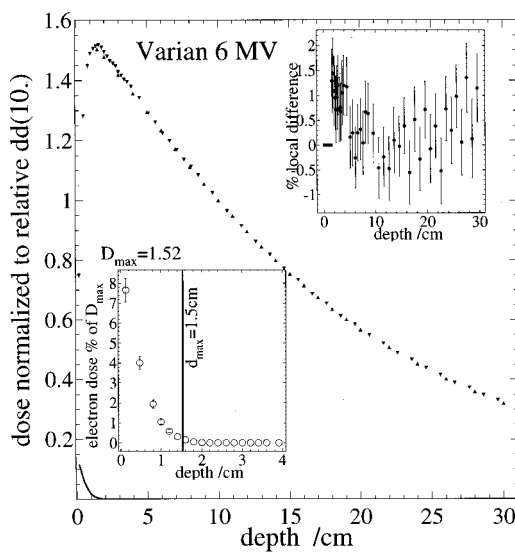


FIG. 2. Comparison of the calculated (using a 0.2 cm FWHM, 5.7 MeV electron beam with 3% FWHM energy spread) (\blacktriangledown) and the measured (\blacktriangle) central-axis depth-dose data for the 6 MV photon beam of the Varian high-energy accelerator. Otherwise as in Fig. 1.

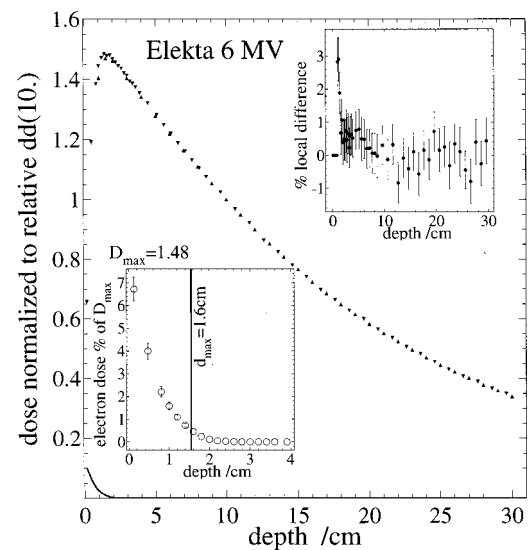


FIG. 4. Comparison of the calculated (using a 0.11 cm FWHM, 6.3 MeV electron beam with 17% FWHM energy spread) (\blacktriangledown) and the measured (\blacktriangle) central-axis depth-dose data for the 6 MV photon beam of the Elekta SL25 6 MV accelerator. Measured data are from Palta *et al.* (Ref. 30). Otherwise as in Fig. 1.

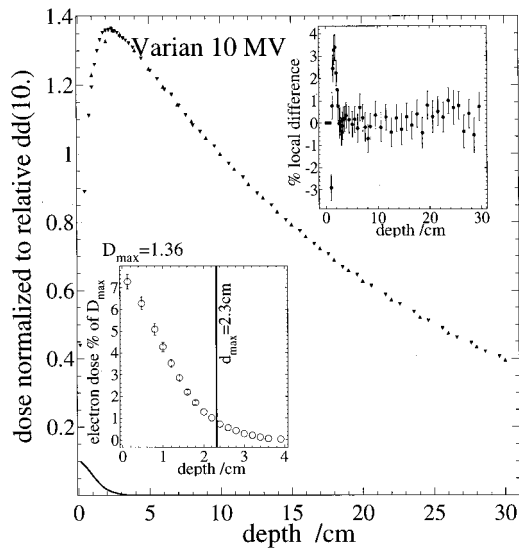


FIG. 5. Comparison of the calculated (using a 0.15 cm FWHM, 10.5 MeV electron beam with 3% FWHM energy spread) (∇) and the measured (\blacktriangle) central-axis depth-dose data for the 10 MV photon beam of the Varian high-energy accelerator. Otherwise as in Fig. 1.

that the calculated and the measured data agree within 1% of local dose, for statistics of about 1% (1σ level), at all depths past depth of maximum dose for all beams, except the 4 MV beam from Varian, where the agreement is slightly worse at larger depths but it is still better than 1.5% of the local dose and much less than 1% of maximum dose. In a previous paper²³ we have shown how correcting for the effective point of measurement of the ion chamber can improve the agreement between calculated and measured depth-dose data in the build-up region. It is not clear whether or not the com-

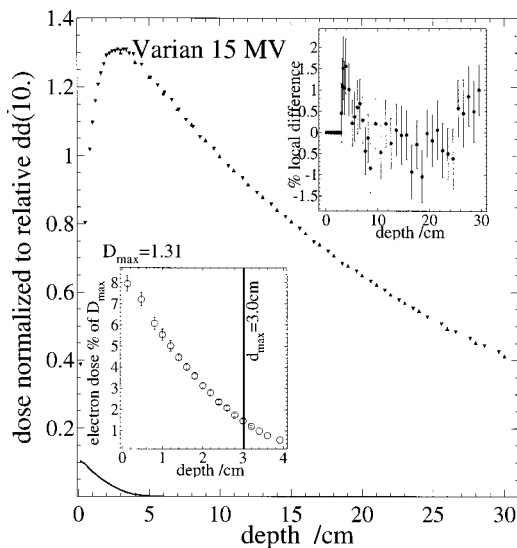


FIG. 6. Comparison of the calculated (using a 0.17 cm FWHM, 14.5 MeV electron beam with 3% FWHM energy spread) (∇) and the measured (\blacktriangle) central-axis depth-dose data for the 15 MV photon beam of the Varian high-energy accelerator. Otherwise as in Fig. 1.

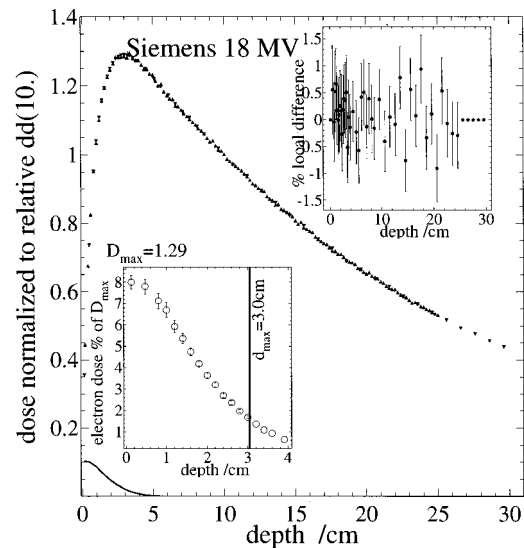


FIG. 7. Comparison of the calculated (using a 0.1 cm FWHM, 14.68 MeV electron beam with an energy spread of 7% HWHM on the LHS of the peak and 1.5% HWHM on the RHS of the peak) (∇) and the measured (\blacktriangle) central-axis depth-dose data for the 18 MV photon beam of the Siemens KD accelerator. Measured data are provided by Dr. Alf Siochi, Siemens Oncology Systems, since TG-46 lacked % dd data for this beam. Otherwise as in Fig. 1.

pared depth-dose data of TG-46²² are corrected for the effective point of measurement, so no further attempt is made to reduce the discrepancy in the build-up region. Furthermore, the excellent agreement between the calculated and the measured depth-dose values for the Siemens 18 MV beam (which were known to be corrected for the effective point of measurement) shows that a good match at all depths is possible, provided that the data are measured carefully.

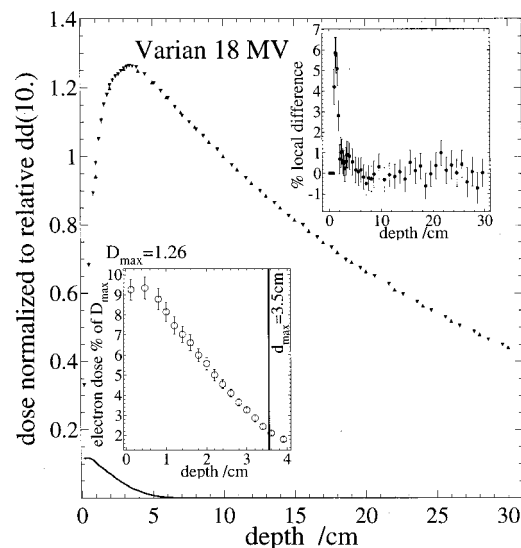


FIG. 8. Comparison of the calculated (using a 0.11 cm FWHM, 18.3 MeV electron beam with 3% FWHM energy spread) (∇) and the measured (\blacktriangle) central-axis depth dose data for the 18 MV photon beam of the Varian high-energy accelerator. Otherwise as in Fig. 1.

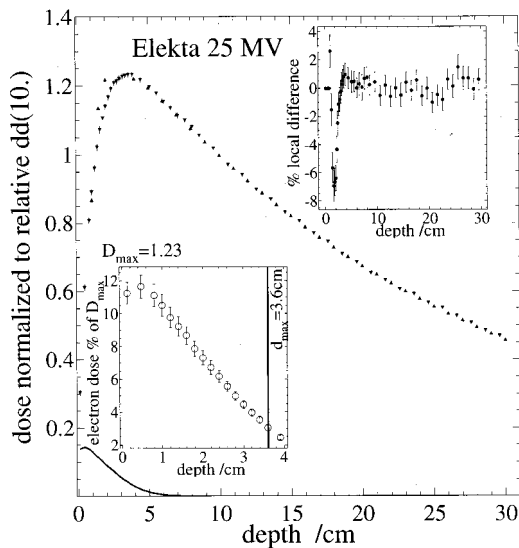


FIG. 9. Comparison of the calculated (using a 0.1 cm FWHM, 19.0 MeV electron beam with 5% FWHM, energy spread) (\blacktriangledown) and the measured (\blacktriangle) central-axis depth-dose data for the 25 MV photon beam of the Elekta SL25 accelerator. Measured data are from Palta *et al.* (Ref. 30). Otherwise as in Fig. 1.

Statistical noise limits the size of the bins used to calculate central-axis depth-dose curves using the Monte Carlo technique. Consequently the depth of the central-axis maximum dose and its value are affected by statistical fluctuations. To obtain a better estimate for the depth of maximum dose, a quadratic fit to the 5 points around and including the bin with the maximum content is used. The value of maximum dose (D_{max}) obtained from this fit is within 0.5% of the value of the bin with maximum content (with better than 0.6% statistics) for all the beams except the 4 MV beam,

where the difference is 3%. In the calculation of $\%dd(10)$, the value of the maximum bin content is used but the reported position of the dose maximum is determined by the fit.

Figures 1–9 also show the contribution to dose from contaminant electrons (solid lines). This contribution is depicted as the percentage of maximum dose in the lower-left insets in Figs. 1–9 and summarized in columns 6 and 7 of Table I. The reliability of the BEAM code in calculating the electron contamination dose has been shown before for high energy photon beams²³ and for ^{60}Co beams.²⁴ Thus the accuracy of the calculated electron contamination is based on the accuracy of our knowledge of the description of the accelerator.

The dose calculation ran at 1.26×10^7 incident electrons/hour on each 200 MHz Pentium Pro at 4 MV, and 1.11×10^7 incident electrons/hour at 25 MV. A summary of calculated depth-dose characteristics is also presented in Table I and discussed in the next section.

B. The photon component and the electron contamination

The report of the AAPM’s task group 51 (TG-51)²⁵ provides a general formula to calculate $\%dd(10)_x$, the photon component of the percentage depth-dose at 10 cm for a $10 \times 10 \text{ cm}^2$ field (specified at the surface) from the value of the measured total percentage depth-dose [$\%dd(10)$] (i.e., one which also has electron contamination) using the formula (for $\%dd(10)$ greater than 75%):²⁶

$$\%dd(10)_x = 1.2667(\%dd(10)) - 20. \tag{1}$$

For beams with energy 10 MV or lower, the calculations show there is typically 0.7% or slightly less electron contamination at depth of dose maximum, and hence $\%dd(10)_x$

TABLE I. Central-axis depth-dose characteristics (for $10 \times 10 \text{ cm}^2$ fields) of the nine realistic photon beams studied here. The Varian linacs are divided into low-energy (LE) and high-energy (HE) linacs by the manufacturer. NAP is the nominal accelerating potential, $\%dd(0)_x$ is the percentage surface dose from photons only, $\%dd_e(0)$ is the electron contamination dose at the surface, $\%dd_e(d_{max})$ is the electron contamination dose at depth of maximum dose, $\%dd_e(10)$ is the calculated value of dose at 10 cm depth, and $\%dd_m(10)$ is the measured value of dose at 10 cm depth. The $\%dd(0)_x$ and $\%dd_e(0)$ values are averaged in the first slab which is 0.25 cm thick, whereas the value of $\%dd_e(d_{max})$ is averaged in a 0.2 cm thick slab. The $\%dd_e(10)$ and $\%dd_m(10)$ values are calculated from fourth order polynomial fits to the fall-off region of the $\%dd$ curve. The maximum dose (D_{max}) in the calculation of $\%dd$ values is obtained from the bin with the maximum content, however the depth of maximum dose (d_{max}) is derived from the location of the peak of a quadratic fit to the five data points surrounding and inclusive of the maximum dose. Depth-dose is calculated in an on-axis cylinder of radius 1.0 cm. The uncertainty in the depth of maximum dose (d_{max}) is 0.1 cm. The uncertainty in maximum dose (D_{max}), based on a 0.2 cm thick bin for its calculation, is estimated to be 0.9% for the 4 MV beam and 0.5% for the 25 MV beam.

Linac	NAP (MV)	d_{max} (cm)	$D_{max} \times 10^{17}$ (Gy/inc. e^-)	$\%dd(0)_x$ (%)	$\%dd_e(0)$ (%)	$\%dd_e(d_{max})$ (%)	$\%dd_e(10)$ (%)	$\%dd_m(10)$ (%)
Varian Clinac LE	4	0.9	3.1 ± 0.03	51 ± 1	5.7 ± 0.7	0.5 ± 0.1	62.6 ± 0.6	63.1 ± 0.3
	6	1.5	10.7 ± 0.04	42 ± 1	7.7 ± 0.6	0.16 ± 0.03	65.9 ± 0.3	66.6 ± 0.3
Varian Clinac HE	10	2.3	29.5 ± 0.1	25.0 ± 0.5	7.3 ± 0.3	0.73 ± 0.05	73.4 ± 0.3	73.6 ± 0.4
	15	3.0	72.4 ± 0.3	21.6 ± 0.5	8.0 ± 0.4	1.7 ± 0.09	76.4 ± 0.3	76.9 ± 0.4
	18	3.5	92.8 ± 0.4	16.9 ± 0.7	9.3 ± 0.5	2.4 ± 0.2	79.1 ± 0.3	79.7 ± 0.4
Elekta SL25	6	1.5	11.2 ± 0.04	38 ± 1	6.7 ± 0.5	0.7 ± 0.1	67.4 ± 0.3	68.1 ± 0.2
	25	3.6	64.7 ± 0.4	13 ± 1	11.2 ± 0.7	2.45 ± 0.1	81.1 ± 0.5	81.7 ± 0.2
Siemens KD	6	1.6	19.3 ± 0.1	39 ± 1	6.3 ± 0.5	0.6 ± 0.1	67.2 ± 0.5	67.7 ± 0.3
	18	3.0	76.0 ± 0.4	19.6 ± 0.5	8.0 ± 0.3	1.7 ± 0.1	77.5 ± 0.4	77.3 ± 0.4

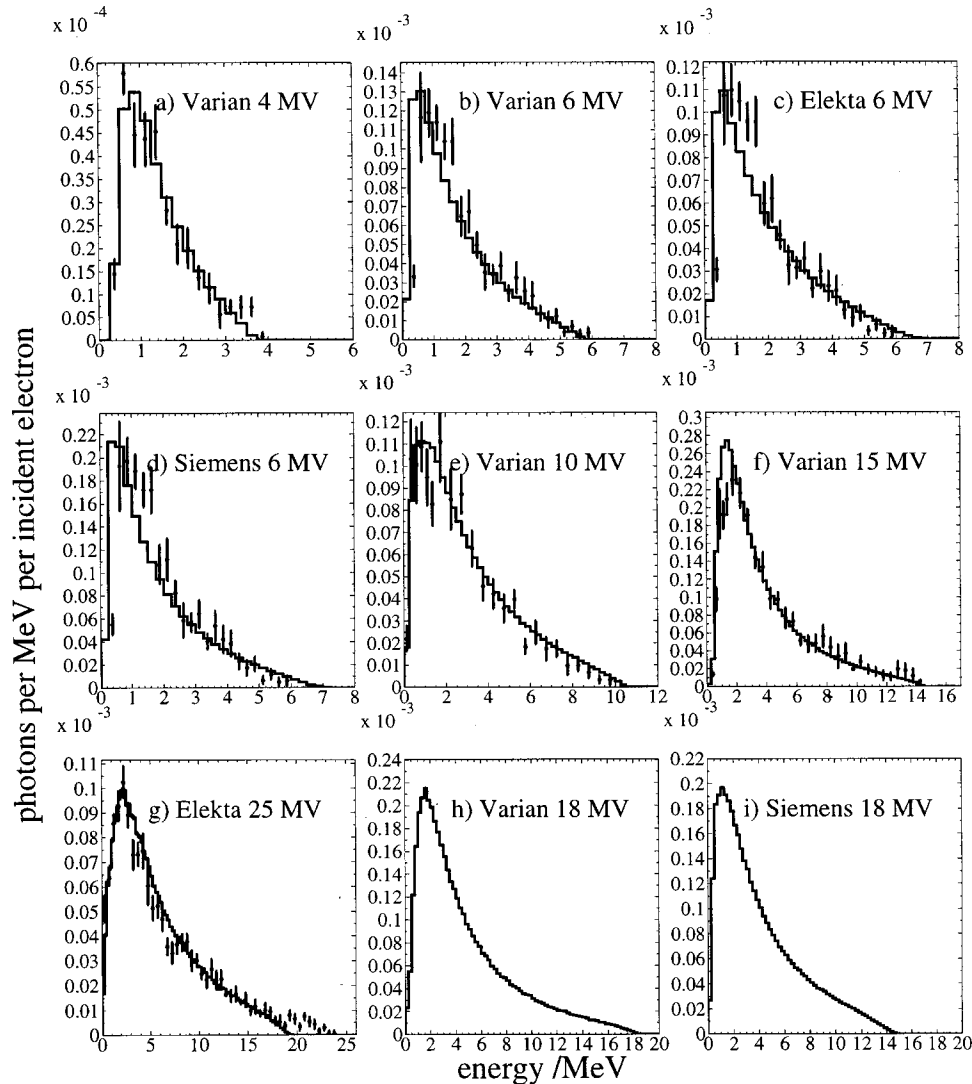


FIG. 10. Comparison of the photon spectra calculated here (histograms) with those previously published by Mohan *et al.* (Ref. 20) (dots with error bars) for Varian machines. Each of Mohan's spectra is normalized to the area under the corresponding calculated spectrum. The Mohan *et al.* data are for the region $0 \leq r \leq 3$ cm, and the current results correspond to $0 \leq r \leq 2.25$ cm. Panel (g) shows a comparison of the 25 MV beam of an Elekta SL25 machine with a 24 MV beam of a Varian machine. Since Mohan *et al.* had no 18 MV beam, no comparison is made at this energy. The spectra are tabulated in Tables II–IV.

will typically be 0.5% less than $\%dd(10)$, contrary with the assertion in TG-51 that $\%dd(10)_x = \%dd(10)$ for such lower-energy beams. For higher-energy beams the % differences $[(TG-51 - \text{value here})/TG-51]$ in the calculated values of $\%dd(10)_x$ are as follows: -0.5% (for the 15 MV beam), -0.4% (for Siemens KD 18 MV beam), -0.7% (for Varian 18 MV beam), and -0.5% (for Elekta 25 MV beam). In all cases the simple formula overestimates the effect of electron contamination, however it is always within 0.7%, i.e., well within the 2% accuracy claimed.

III. ANALYSIS OF SPECTRA

A. Comparison of photon spectra with Mohan *et al.*

Figure 10 compares photon spectra (number of photons per MeV per incident electron on the target) obtained in this work, with spectra (number of photons per MeV) published

by Mohan *et al.*²⁰ Each of the Mohan *et al.* spectra is normalized to the area of the corresponding spectrum calculated in this work. The uncertainty in the calculated photon fluence on the central axis (in the radial bin, $0 \leq r \leq 2.25$ cm) in the 4 MV simulation is 0.2% and in the 25 MV simulation is 0.4%. The Varian machines used in the two studies are similar yet different. There are small differences in the thickness of the targets and their backings, but only for the 4 and the 6 MV beams. Also, the material of the flattening filters used in the two studies are different at 6 and 10 MV. Differences in the average photon energies are discussed in the next section. For the purpose of comparison, panels (c), (d), and (g) compare Mohan's spectra, with the spectra calculated in this work for corresponding energies but produced by linacs made by other manufacturers. Mohan's data lack an 18 MV beam, therefore panels (h) and (i), only present the spectra calculated in this work.

TABLE II. Photon fluence spectra (photons per MeV per incident electron) of the 15–25 MV beams, as shown in Fig. 10 for the radial bin $0 \leq r \leq 2.5$ cm. The bins are 250 keV wide, and the fluence data are tabulated with the energy at the end of each bin. The percentage uncertainty in each bin is presented in parentheses. The spectra are continued in Table III.

E (MeV)	Elekta (25 MV)	Varian (18 MV)	Siemens (18 MV)	Varian (15 MV)
0.250	0.167E-04(3.2%)	0.235E-04(2.43%)	0.268E-04(1.64%)	0.297E-05(4.34%)
0.500	0.406E-04(2.3%)	0.552E-04(1.55%)	0.124E-03(0.69%)	0.310E-04(1.25%)
0.750	0.620E-04(1.8%)	0.122E-03(0.96%)	0.184E-03(0.56%)	0.151E-03(0.54%)
1.000	0.680E-04(1.7%)	0.164E-03(0.78%)	0.191E-03(0.51%)	0.232E-03(0.41%)
1.250	0.790E-04(1.4%)	0.194E-03(0.70%)	0.197E-03(0.49%)	0.267E-03(0.37%)
1.500	0.868E-04(1.3%)	0.207E-03(0.66%)	0.191E-03(0.48%)	0.275E-03(0.37%)
1.750	0.924E-04(1.2%)	0.215E-03(0.66%)	0.186E-03(0.47%)	0.264E-03(0.37%)
2.000	0.964E-04(1.1%)	0.205E-03(0.64%)	0.178E-03(0.47%)	0.246E-03(0.38%)
2.250	0.992E-04(1.1%)	0.199E-03(0.65%)	0.167E-03(0.47%)	0.226E-03(0.39%)
2.500	0.993E-04(1.1%)	0.186E-03(0.66%)	0.159E-03(0.48%)	0.206E-03(0.40%)
2.750	0.933E-04(1.0%)	0.177E-03(0.66%)	0.148E-03(0.49%)	0.186E-03(0.41%)
3.000	0.933E-04(1.0%)	0.166E-03(0.68%)	0.138E-03(0.48%)	0.170E-03(0.43%)
3.250	0.890E-04(1.0%)	0.155E-03(0.70%)	0.131E-03(0.50%)	0.156E-03(0.44%)
3.500	0.880E-04(1.1%)	0.144E-03(0.70%)	0.121E-03(0.50%)	0.142E-03(0.45%)
3.750	0.818E-04(1.0%)	0.133E-03(0.73%)	0.114E-03(0.51%)	0.129E-03(0.47%)
4.000	0.805E-04(1.0%)	0.127E-03(0.74%)	0.107E-03(0.52%)	0.118E-03(0.49%)
4.250	0.785E-04(1.1%)	0.119E-03(0.78%)	0.101E-03(0.54%)	0.108E-03(0.50%)
4.500	0.744E-04(1.1%)	0.110E-03(0.78%)	0.938E-04(0.54%)	0.101E-03(0.52%)
4.750	0.714E-04(1.0%)	0.105E-03(0.82%)	0.887E-04(0.56%)	0.919E-04(0.54%)
5.000	0.682E-04(1.1%)	0.961E-04(0.83%)	0.834E-04(0.57%)	0.852E-04(0.56%)
5.250	0.644E-04(1.0%)	0.916E-04(0.84%)	0.788E-04(0.59%)	0.788E-04(0.57%)
5.500	0.603E-04(1.1%)	0.860E-04(0.88%)	0.744E-04(0.58%)	0.726E-04(0.59%)
5.750	0.578E-04(1.1%)	0.809E-04(0.88%)	0.696E-04(0.61%)	0.675E-04(0.62%)
6.000	0.562E-04(1.1%)	0.769E-04(0.90%)	0.659E-04(0.62%)	0.627E-04(0.63%)
6.250	0.537E-04(1.2%)	0.709E-04(0.94%)	0.630E-04(0.63%)	0.585E-04(0.65%)
6.500	0.503E-04(1.2%)	0.682E-04(0.94%)	0.590E-04(0.66%)	0.552E-04(0.66%)
6.750	0.487E-04(1.1%)	0.646E-04(0.98%)	0.558E-04(0.65%)	0.512E-04(0.68%)
7.000	0.465E-04(1.2%)	0.595E-04(0.99%)	0.526E-04(0.67%)	0.480E-04(0.71%)
7.250	0.439E-04(1.2%)	0.569E-04(1.01%)	0.509E-04(0.68%)	0.457E-04(0.72%)
7.500	0.423E-04(1.2%)	0.533E-04(1.06%)	0.477E-04(0.69%)	0.428E-04(0.73%)
7.750	0.403E-04(1.2%)	0.502E-04(1.04%)	0.460E-04(0.72%)	0.396E-04(0.75%)
8.000	0.396E-04(1.2%)	0.495E-04(1.10%)	0.431E-04(0.74%)	0.374E-04(0.78%)
8.250	0.375E-04(1.3%)	0.469E-04(1.11%)	0.410E-04(0.75%)	0.354E-04(0.79%)
8.500	0.369E-04(1.2%)	0.434E-04(1.15%)	0.386E-04(0.77%)	0.332E-04(0.82%)
8.750	0.344E-04(1.3%)	0.418E-04(1.16%)	0.365E-04(0.79%)	0.314E-04(0.86%)

Tables II, III and IV present tabulated photon spectra. The precision of the calculated fluence spectra for all the beams used in the dose calculations is high, the uncertainty in each 250 keV wide bin is usually between 1 and 4%, except for the high-energy end of the spectra. Note that the spectra extend above the mean energy of the incident electron beams due to the width of the incident beam's energy distribution.

Figure 11 compares the three 6 MV photon spectra calculated in this work. The ratios of the spectra of Siemens and Elekta 6 MV beams to that of Varian shows that the Siemens beam produces more photons per incident electron than Varian or Elekta at this energy. The spectral shapes are somewhat similar. The differences at the high-energy end are caused by the differences in the mean incident electron energies and their spreads (see paper I).

B. Average energy distribution

Figure 12 shows the calculated average energies at 100 cm SSD in large open fields for all the beams studied. For

comparison, values calculated by Mohan *et al.*²⁰ for Varian machines are also shown as filled circles. The average energy distributions are also decomposed to show the total (solid histograms), direct (dashed histograms), and scattered photon (dotted histograms) components. Direct photons are those which have not interacted anywhere past the target before reaching the scoring plane. The agreement between our calculated values of the average photon energy and those of Mohan *et al.* is quite good for the 4 and the 15 MV beams of the Varian machines, despite spectral differences (see Fig. 10). The calculated values of the average energy for the 6 MV beam are lower and for the 10 MV beam are higher than those calculated by Mohan *et al.*²⁰ However, the match obtained for both off-axis factors and relative depth-dose indicate that the energy of the electron beam incident on the target for the 6 and 10 MV beams, cannot be dramatically different from those used in this work (i.e., 5.7 MeV and 10.5 MeV). Mohan *et al.*²⁰ calculated TMR values which overestimate the measured values at 6 MV and underestimate

TABLE III. Continuation of Table II.

E (MeV)	Elekta (25 MV)	Varian (18 MV)	Siemens (18 MV)	Varian (15 MV)
9.000	0.332E-04(1.3%)	0.401E-04(1.16%)	0.353E-04(0.80%)	0.297E-04(0.88%)
9.250	0.317E-04(1.4%)	0.377E-04(1.22%)	0.337E-04(0.81%)	0.275E-04(0.89%)
9.500	0.306E-04(1.4%)	0.353E-04(1.23%)	0.318E-04(0.84%)	0.264E-04(0.92%)
9.750	0.294E-04(1.4%)	0.345E-04(1.23%)	0.303E-04(0.86%)	0.245E-04(0.96%)
10.000	0.280E-04(1.4%)	0.339E-04(1.30%)	0.284E-04(0.87%)	0.231E-04(0.98%)
10.250	0.276E-04(1.4%)	0.310E-04(1.31%)	0.272E-04(0.90%)	0.217E-04(1.00%)
10.500	0.269E-04(1.5%)	0.296E-04(1.39%)	0.254E-04(0.95%)	0.204E-04(1.04%)
10.750	0.253E-04(1.5%)	0.282E-04(1.39%)	0.239E-04(0.96%)	0.196E-04(1.05%)
11.000	0.235E-04(1.5%)	0.268E-04(1.42%)	0.228E-04(0.98%)	0.182E-04(1.10%)
11.250	0.235E-04(1.5%)	0.254E-04(1.45%)	0.213E-04(1.01%)	0.163E-04(1.16%)
11.500	0.225E-04(1.6%)	0.244E-04(1.45%)	0.202E-04(1.04%)	0.155E-04(1.20%)
11.750	0.209E-04(1.6%)	0.234E-04(1.52%)	0.185E-04(1.09%)	0.145E-04(1.21%)
12.000	0.204E-04(1.6%)	0.222E-04(1.57%)	0.168E-04(1.13%)	0.133E-04(1.27%)
12.250	0.185E-04(1.7%)	0.210E-04(1.57%)	0.157E-04(1.18%)	0.124E-04(1.30%)
12.500	0.190E-04(1.7%)	0.206E-04(1.59%)	0.143E-04(1.20%)	0.115E-04(1.36%)
12.750	0.186E-04(1.7%)	0.201E-04(1.65%)	0.126E-04(1.30%)	0.102E-04(1.46%)
13.000	0.174E-04(1.8%)	0.186E-04(1.70%)	0.113E-04(1.37%)	0.902E-05(1.51%)
13.250	0.171E-04(1.8%)	0.175E-04(1.77%)	0.972E-05(1.45%)	0.817E-05(1.61%)
13.500	0.159E-04(1.9%)	0.166E-04(1.76%)	0.812E-05(1.61%)	0.700E-05(1.71%)
13.750	0.158E-04(1.8%)	0.161E-04(1.78%)	0.625E-05(1.83%)	0.585E-05(1.87%)
14.000	0.149E-04(1.8%)	0.153E-04(1.85%)	0.500E-05(2.09%)	0.451E-05(2.12%)
14.250	0.141E-04(1.9%)	0.149E-04(1.87%)	0.324E-05(2.60%)	0.273E-05(2.73%)
14.500	0.139E-04(1.9%)	0.140E-04(1.91%)	0.194E-05(3.23%)	0.137E-05(3.85%)
14.750	0.131E-04(2.0%)	0.127E-04(2.00%)	0.706E-06(5.36%)	0.306E-06(8.14%)
15.000	0.124E-04(2.1%)	0.125E-04(2.05%)	0.104E-06(14.00%)	0.265E-07(27.74%)
15.250	0.115E-04(2.1%)	0.118E-04(2.12%)	0.418E-08(70.71%)	
15.500	0.114E-04(2.1%)	0.105E-04(2.24%)		
15.750	0.108E-04(2.2%)	0.106E-04(2.22%)		
16.000	0.999E-05(2.3%)	0.953E-05(2.34%)		
16.250	0.917E-05(2.4%)	0.898E-05(2.38%)		
16.500	0.888E-05(2.4%)	0.825E-05(2.48%)		
16.750	0.858E-05(2.5%)	0.715E-05(2.66%)		
17.000	0.790E-05(2.5%)	0.653E-05(2.78%)		
17.250	0.703E-05(2.7%)	0.544E-05(3.05%)		
17.500	0.591E-05(2.9%)	0.439E-05(3.39%)		
17.750	0.529E-05(3.1%)	0.366E-05(3.72%)		
18.000	0.503E-05(3.3%)	0.237E-05(4.61%)		
18.250	0.392E-05(3.8%)	0.125E-05(6.35%)		
18.500	0.291E-05(4.2%)	0.363E-06(11.79%)		
18.750	0.207E-05(4.9%)	0.657E-07(27.74%)		
19.000	0.119E-05(6.5%)			
19.250	0.584E-06(9.3%)			
19.500	0.217E-06(15.3%)			
19.750	0.958E-07(22.9%)			
20.000	0.101E-07(70.7%)			

measured values at 10 MV, supporting the fact that the incident energy assumed by them is higher (for the 6 MV beam) and lower (for the 10 MV beam) than it should be, in agreement with our findings. Panels (d), (e), and (f) of Fig. 12, show an intercomparison of average energies for the same nominal accelerating potential (6 MV) produced by the three different manufacturers. It can be seen that the differences in the calculated average energies of the photon beams produced by the three linacs are consistent with the spectral differences presented in Fig. 11. Both Siemens KD beams [see panels (e) and (h) of Fig. 12] exhibit a dip in the average energy at large distances from the axis. The dip is due to the projection of the flattening filter not covering the entire field,

as discussed by Faddegon *et al.*²⁷ for Siemens MXE and MDX linacs. Finally, panel (i) of Fig. 12 compares an Elekta SL25 25 MV photon beam with a 24 MV beam calculated by Mohan *et al.*²⁰ for a Varian machine.

C. Photon energy-fluence spectra

Figures 13, 14, and 15 show the energy-weighted photon spectra averaged over a 10×10 cm² field, as opposed to the central axis fluence spectra (not energy-weighted) shown in Fig. 10. For most of the beams, 94 to 97% of the photons are direct (i.e., they have only interacted in the target, before reaching the scoring plane at 100 cm). The Elekta 25 MV

TABLE IV. 4–10 MV photon fluence spectra (photons per MeV per incident electron), for the radial bin $0 \leq r \leq 2.5$ cm, as shown in Fig. 10. the bins are 250 keV wide, and the fluence data are tabulated with the energy at the end of each bin. The uncertainty in each bin is presented in parentheses.

E (MeV)	Varian (10 MV)	Varian (6 MV)	Siemens (6 MV)	Elekta (6 MV)	Varian (4 MV)
0.250	0.181E-04(1.30%)	0.214E-04(1.0%)	0.422E-04(1.13%)	0.173E-04(1.5%)	0.853E-07(14.83%)
0.500	0.845E-04(0.53%)	0.126E-03(0.4%)	0.214E-03(0.44%)	0.100E-03(0.5%)	0.167E-04(0.90%)
0.750	0.109E-03(0.45%)	0.131E-03(0.3%)	0.210E-03(0.41%)	0.110E-03(0.5%)	0.501E-04(0.50%)
1.000	0.111E-03(0.43%)	0.114E-03(0.3%)	0.176E-03(0.43%)	0.952E-04(0.5%)	0.542E-04(0.46%)
1.250	0.111E-03(0.43%)	0.976E-04(0.4%)	0.149E-03(0.46%)	0.827E-04(0.5%)	0.472E-04(0.48%)
1.500	0.109E-03(0.43%)	0.836E-04(0.4%)	0.127E-03(0.48%)	0.721E-04(0.5%)	0.391E-04(0.53%)
1.750	0.102E-03(0.44%)	0.725E-04(0.4%)	0.109E-03(0.52%)	0.635E-04(0.5%)	0.314E-04(0.57%)
2.000	0.949E-04(0.44%)	0.623E-04(0.4%)	0.946E-04(0.54%)	0.557E-04(0.5%)	0.249E-04(0.63%)
2.250	0.879E-04(0.45%)	0.535E-04(0.5%)	0.815E-04(0.57%)	0.493E-04(0.5%)	0.191E-04(0.70%)
2.500	0.813E-04(0.46%)	0.459E-04(0.5%)	0.711E-04(0.60%)	0.437E-04(0.6%)	0.154E-04(0.77%)
2.750	0.750E-04(0.47%)	0.395E-04(0.5%)	0.624E-04(0.64%)	0.386E-04(0.6%)	0.116E-04(0.88%)
3.000	0.689E-04(0.49%)	0.347E-04(0.5%)	0.549E-04(0.66%)	0.345E-04(0.6%)	0.875E-05(0.99%)
3.250	0.635E-04(0.50%)	0.298E-04(0.6%)	0.481E-04(0.69%)	0.302E-04(0.6%)	0.604E-05(1.15%)
3.500	0.588E-04(0.51%)	0.261E-04(0.6%)	0.430E-04(0.73%)	0.270E-04(0.7%)	0.364E-05(1.46%)
3.750	0.542E-04(0.52%)	0.225E-04(0.6%)	0.380E-04(0.75%)	0.240E-04(0.7%)	0.113E-05(2.43%)
4.000	0.500E-04(0.53%)	0.191E-04(0.7%)	0.336E-04(0.81%)	0.210E-04(0.7%)	0.836E-08(25.79%)
4.250	0.465E-04(0.56%)	0.166E-04(0.7%)	0.294E-04(0.83%)	0.186E-04(0.8%)	
4.500	0.430E-04(0.57%)	0.138E-04(0.8%)	0.261E-04(0.90%)	0.164E-04(0.8%)	
4.750	0.396E-04(0.59%)	0.114E-04(0.8%)	0.228E-04(0.94%)	0.142E-04(0.9%)	
5.000	0.364E-04(0.61%)	0.904E-05(0.9%)	0.199E-04(0.97%)	0.121E-04(0.9%)	
5.250	0.342E-04(0.62%)	0.655E-05(1.0%)	0.171E-04(1.04%)	0.101E-04(1.0%)	
5.500	0.318E-04(0.64%)	0.409E-05(1.3%)	0.146E-04(1.13%)	0.817E-05(1.1%)	
5.750	0.289E-04(0.66%)	0.140E-05(2.2%)	0.120E-04(1.21%)	0.645E-05(1.2%)	
6.000	0.274E-04(0.68%)	0.434E-07(11.4%)	0.965E-05(1.33%)	0.455E-05(1.4%)	
6.250	0.254E-04(0.70%)		0.709E-05(1.52%)	0.300E-05(1.8%)	
6.500	0.236E-04(0.73%)		0.471E-05(1.92%)	0.156E-05(2.4%)	
6.750	0.216E-04(0.74%)		0.266E-05(2.39%)	0.734E-06(3.4%)	
7.000	0.200E-04(0.77%)		0.130E-05(3.39%)	0.294E-06(5.0%)	
7.250	0.185E-04(0.80%)		0.533E-06(5.01%)	0.882E-07(9.0%)	
7.500	0.171E-04(0.83%)		0.143E-06(9.70%)	0.188E-07(19.8%)	
7.750	0.156E-04(0.87%)		0.292E-07(21.39%)	0.277E-08(50.0%)	
8.000	0.143E-04(0.90%)		0.426E-08(57.76%)	0.159E-08(70.8%)	
8.250	0.132E-04(0.92%)				
8.500	0.119E-04(0.99%)				
8.750	0.106E-04(1.03%)				
9.000	0.917E-05(1.08%)				
9.250	0.803E-05(1.17%)				
9.500	0.668E-05(1.28%)				
9.750	0.553E-05(1.39%)				
10.000	0.408E-05(1.64%)				
10.250	0.253E-05(2.03%)				
10.500	0.998E-06(3.21%)				
10.750	0.120E-06(9.21%)				
11.000	0.307E-08(57.74%)				

beam has the largest number of scattered photons, resulting in about 92% direct photons. The scattered photons are grouped into three major categories: those last scattered from the primary collimator, the flattening filter or the field-defining jaws. Most of the scattered photons appear to originate from (i.e., they scatter for the last time in) the primary collimator or the flattening filter. The scatter contributions from the primary collimator and the flattening filter are typically between 1 and 4.5% each. Some of the high energy beams (Siemens 18 MV and Elekta 25 MV) have beam hardeners inserted in the primary collimator and therefore their fraction of scattered energy fluence from the primary collimator structure is noticeably higher than those without the hardener (Varian 18 MV). The jaws are responsible for 0.2%

and 0.3% of the scattered energy fluence in all the beams. Reducing the thickness of the jaws by half, increases the contribution to scattered energy fluence by about a factor of 3 to 4. There may be other structures, besides the target, the primary collimator, the flattening filter and the jaws, which the beam passes through and may interact with. The scatter from those additional structures is generally much less than 1% in total, and is not explicitly depicted in Figs. 13–15 or Table V. The spectral shapes of the scatter components at different energies (4 to 18 MV) of the same linac (Varian) are generally similar.

The classification of photon scatter from different component modules in BEAM, can be done using LATCH²¹ or alternatively using ZLAST.²⁸ There are advantages and dis-

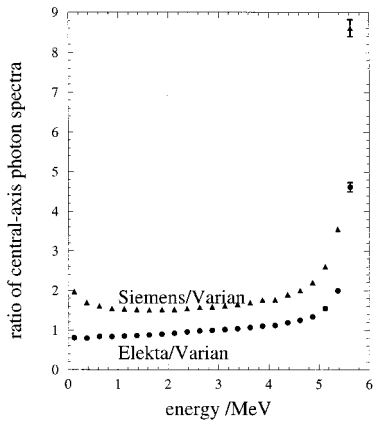


FIG. 11. Ratio of central-axis photon spectra of Siemens and Elekta 6 MV beams to that of Varian. The 6 MV Elekta and Siemens beams extend to 8 MeV, because of higher incident energies and broader incident spectra, but the ratios end at 6 MeV where the Varian spectrum goes to zero.

advantages associated with either method. The advantage of using LATCH is the simplicity of addressing a certain component module with only one number (the corresponding bit assigned to it in LATCH). The disadvantage, however, is that no distinction can be made as to which module resulted in the final scattering event before the photon reaches the scoring plane. The disadvantage of using ZLAST is that a component module has to be addressed with its extension along the x , y , and z axes. The advantage, however, is that the scattering site from the component module or any part thereof can be reconstructed in 3D and the coordinates of the last interaction before reaching the scoring plane is unambiguously specified. Here we have adopted a hybrid approach and use both ZLAST and LATCH to uniquely specify sources of scatter. This hybrid approach is a must in some beams, where a flattening filter is embedded in the conical opening of the primary collimator, making the distinction

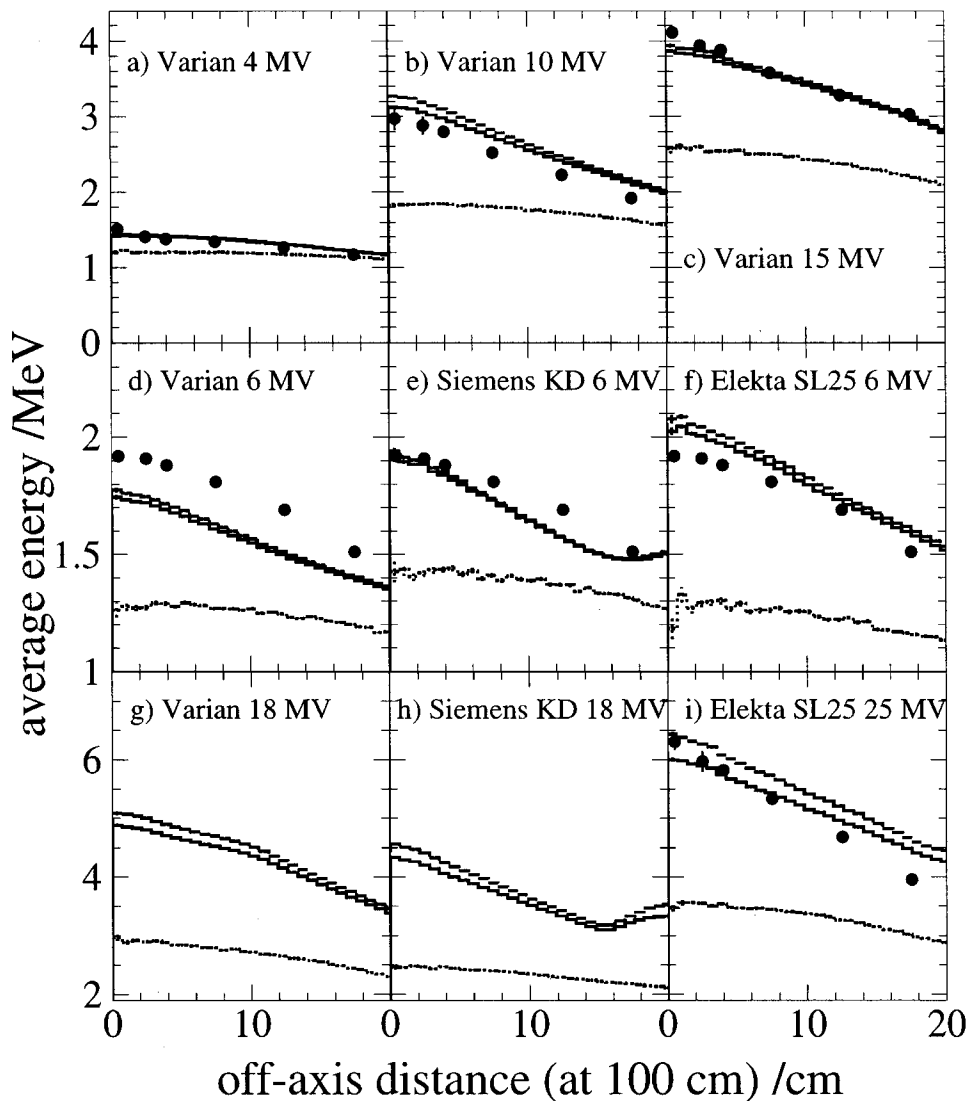


FIG. 12. Calculated average photon energies (above 0.01 MeV) for large open fields at 100 cm, scored in annular bins, for the commercial linacs studied in this work. The filled circles are calculated by Mohan *et al.* (Ref. 20) for Varian Clinacs. The three histograms represent average energies for all photons (solid histograms), direct photons (dashed histograms), and scattered photons (dotted histograms).

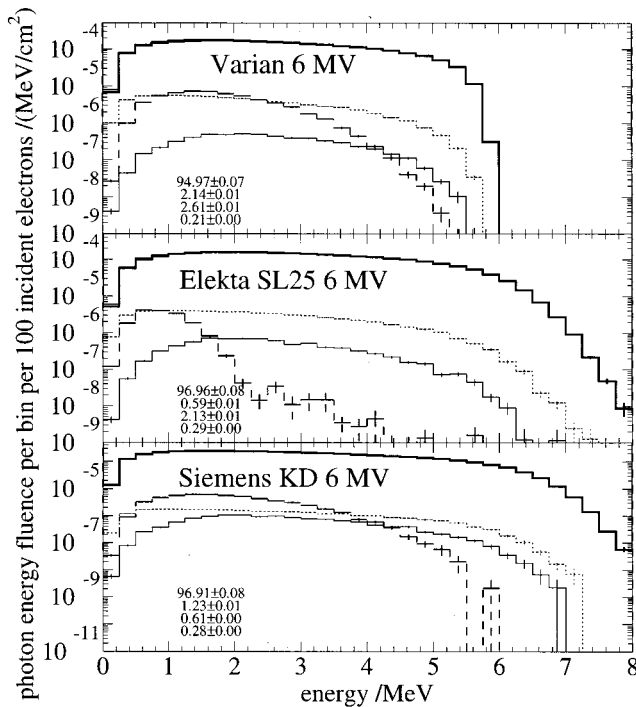


FIG. 13. Photon energy fluence spectra, averaged over a $10 \times 10 \text{ cm}^2$ field. The bin size is 250 keV. The values printed on the lower left of each panel represent the contributions to the energy fluence in percentage from (top to bottom): direct photons (thick solid histogram), photons last scattered in the primary collimator (dashed histogram), photons last scattered in the flattening filter (dotted), and photons last scattered in the jaws (thin solid). Histograms representing total photons are also plotted. However, they can be distinguished from direct photons only in the high-energy beams. The contributions to photon energy fluence are summarized in Table V.

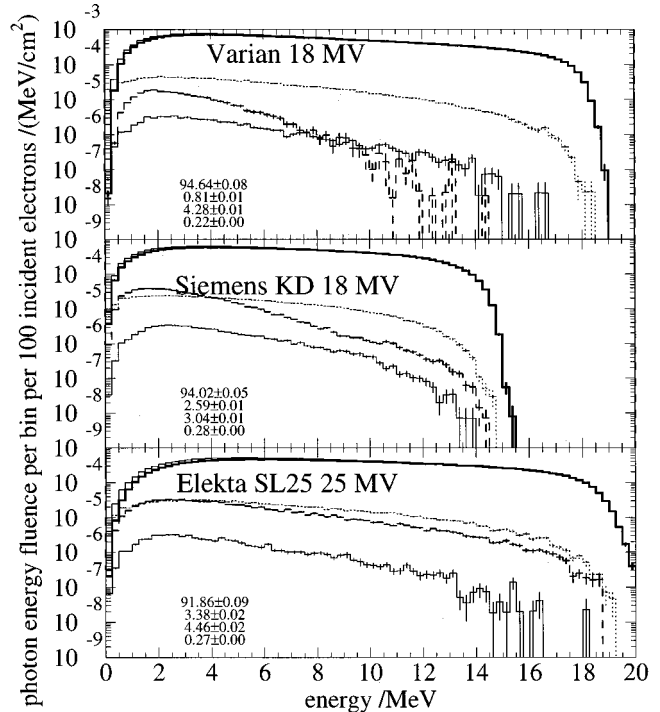


FIG. 15. As in Fig. 13.

between the flattening filter and the primary collimator difficult if one only uses ZLAST.

The contributions of direct and scattered photons to the photon energy fluence for the beams modelled, as well as the corresponding average energies over the entire field are summarized in Table V.

D. Electron contamination fluence spectra

Figure 16 shows the calculated fluence spectra for contaminant electrons reaching a $10 \times 10 \text{ cm}^2$ field at 100 cm. The sudden drop in the fluence of very low-energy electrons is due to the cutoff kinetic energy of 189 keV for the transport of electrons. These spectra remain essentially invariant across the field.

IV. SUMMARY AND CONCLUSIONS

Nine beams from three major medical linac manufacturers, ranging in energy from 4 MV to 25 MV are analyzed in detail. The calculated and measured depth-dose data agree within 1% (local dose), for statistics which are generally better than 0.5% (1σ level), at all depths past depth of maximum dose. The contribution of the electron contamination to the central-axis depth-dose is calculated and at the surface constitutes between 6% of maximum dose for the 4 MV beam and 11% of maximum dose for the 25 MV beam. The calculated values of percentage depth-dose at 10 cm depth for the simulations and the measurements agree well within statistical uncertainties. The calculated central-axis photon spectra have much reduced statistical uncertainties compared to those calculated by Mohan *et al.*²⁰ and show some differences.

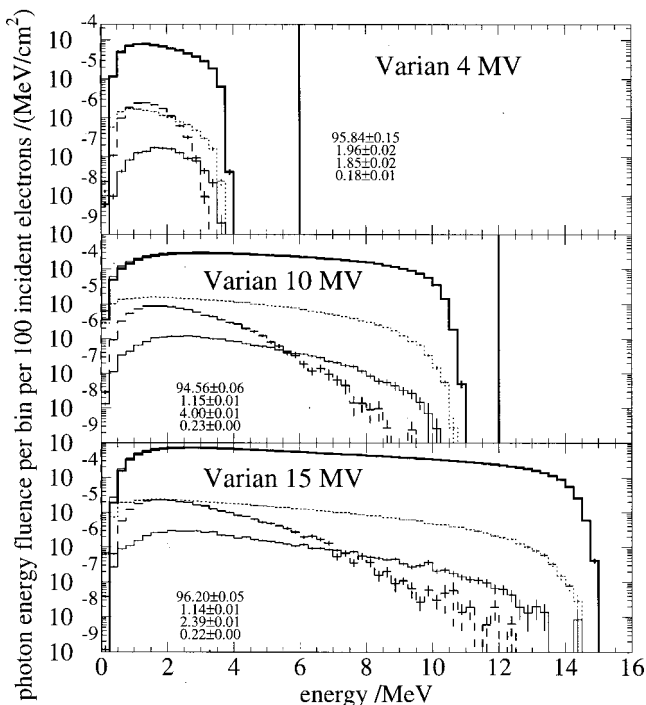


FIG. 14. As in Fig. 13.

TABLE V. Contribution of direct and scattered photons to the photon energy fluence, ψ , in the different beams. The values are for a $10 \times 10 \text{ cm}^2$ field and the corresponding spectra, differential in energy, are plotted in Figs. 13–15. PC represents the primary collimator and FF represents the flattening filter. \bar{E}_A is the average energy of scattered photons of type A reaching the scoring plane at 100 cm, inside the $10 \times 10 \text{ cm}^2$ field and is given by the numbers in square brackets.

Linac	NAP (MV)	Photons per $10^6 \text{ inc } e^-$	ψ_{direct} (%) [\bar{E}_{direct}] (meV)	ψ_{PC} (%) [\bar{E}_{PC}] (MeV)	ψ_{FF} (%) [\bar{E}_{FF}] (MeV)	ψ_{JAW} (%) [\bar{E}_{JAW}] (MeV)
Varian Clinac Low-Energy	4	514 ± 0.4	95.8 ± 0.1 [1.37]	1.96 ± 0.02 [1.25]	1.85 ± 0.01 [1.14]	0.175 ± 0.004 [1.56]
Varian Clinac High-Energy	6	1647 ± 1	94.97 ± 0.07 [1.63]	2.14 ± 0.01 [1.39]	2.61 ± 0.01 [1.16]	0.213 ± 0.003 [1.91]
	10	2869 ± 3	94.56 ± 0.06 [3.04]	1.15 ± 0.01 [1.77]	4.00 ± 0.01 [1.79]	0.234 ± 0.002 [2.44]
	15	6791 ± 5	96.20 ± 0.05 [3.75]	1.14 ± 0.01 [2.04]	2.39 ± 0.01 [2.44]	0.224 ± 0.002 [2.65]
	18	7207 ± 5	94.64 ± 0.08 [4.86]	0.81 ± 0.01 [2.32]	4.28 ± 0.01 [2.71]	0.218 ± 0.003 [2.80]
Elekta SL25	6	1513 ± 1	96.96 ± 0.08 [1.87]	0.600 ± 0.005 [0.75]	2.13 ± 0.01 [1.30]	0.285 ± 0.004 [1.95]
	25	4583 ± 3	91.86 ± 0.09 [6.05]	3.38 ± 0.02 [3.10]	4.46 ± 0.02 [3.11]	0.269 ± 0.003 [2.85]
Siemens KD	6	2530 ± 1	96.91 ± 0.08 [1.76]	1.23 ± 0.01 [1.46]	0.607 ± 0.005 [1.44]	0.282 ± 0.004 [2.08]
	18	6281 ± 2	94.02 ± 0.05 [4.14]	2.58 ± 0.01 [1.95]	3.04 ± 0.01 [2.41]	0.279 ± 0.002 [2.75]

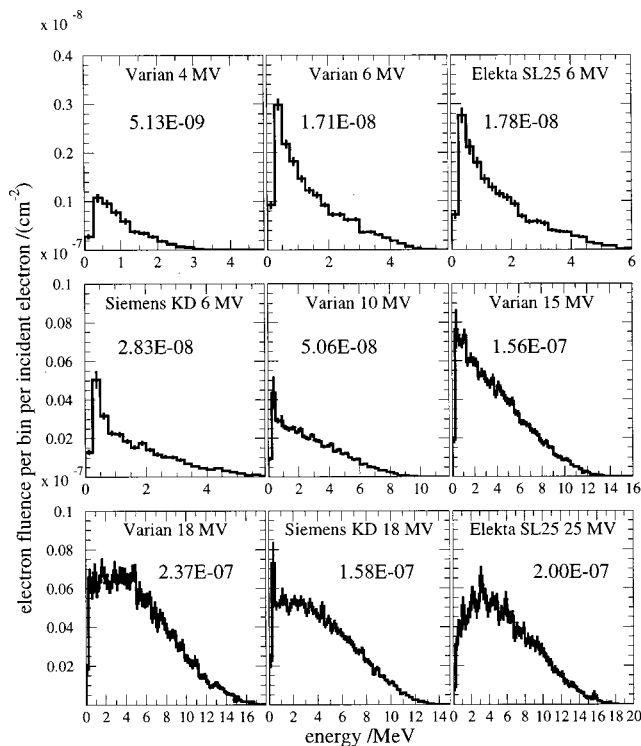


FIG. 16. Fluence spectra of contaminant electrons at 100 cm SSD, averaged inside a $10 \times 10 \text{ cm}^2$ field. The numbers inside the graphs represent the total average electron fluence per incident electron.

At 6 MV, a cross-comparison between the three different linacs is possible. The ratio of the spectra vary dramatically at the high energy end due to differences in the mean incident electron energies and their spreads (see paper I). The Siemens 6 MV beam contains more low- and high-energy photons than the other two beams. The calculated average energies of the photon beams produced by the three linacs also reflect such spectral differences.

The calculated average energies compare well with those of Mohan *et al.* for the 4 and 15 MV beams of Varian machines. But the calculated values of the average energy for the 6 MV beam are lower and those of the 10 MV beam are significantly higher than the calculated values by Mohan *et al.*²⁰ However, for the 10 MV beam for example, the match obtained for both off-axis factors and relative depth-dose indicate that the energy of the electron beam incident on the target cannot be dramatically lower than that used in this work (i.e., 10.5 MeV). Mohan *et al.*'s calculated TMRs²⁰ dramatically underestimate measured values at 10 MV, supporting the fact that the incident energy assumed by them is lower than it should have been.

For most of the beams, 94 to 97 % of the photon energy fluence is direct (i.e., is contributed by photons which have only interacted in the target, before reaching the scoring plane at 100 cm). The Elekta 25 MV beam has the highest number of scattered photons, resulting in about 92% direct-photon energy fluence. The scatter contributions to the energy fluence from the primary collimator and the flattening

filter are typically between 1 and 4.5 % each. The jaws contribute 0.2% to 0.3% to the photon energy fluence in the $10 \times 10 \text{ cm}^2$ fields studied. The scatter from additional structures is less than 1% in total.

ACKNOWLEDGMENTS

We thank Varian, Siemens, and Elekta for providing us with the specifications needed for linac simulations. We thank Dr. Chen-Shou Chui from Memorial Sloan-Kettering Cancer Center for providing us with the photon spectra of the Mohan *et al.* paper,²⁰ CERN for providing us with the PAW²⁹ data analysis software, Dr. Michel Proulx of NRC for his expertise in computer network management and Blake Walters for support of the BEAM system. This work was partially supported by NCI grant R01 CA52692 and by MDS Nordion.

^aOttawa Carleton Institute of Physics, Carleton University, Ottawa, Ontario, K1A 0R6, Canada. Present address: NOMOS Corporation, www.nomos.com

^bElectronic mail: dave@irs.phy.nrc.ca and <http://www.irs.inms.nrc.ca/inms/irs/irs.html>

¹D. Sheikh-Bagheri and D. W. O. Rogers, "Sensitivity of megavoltage photon beam Monte Carlo simulations to electron beam and other parameters," *Med. Phys.* **29**, 379–390 (2002).

²L. B. Levy, R. G. Waggener, W. D. McDavid, and W. H. Payne, "Experimental and calculated bremsstrahlung spectra from a 25-MeV linear accelerator and a 19-MeV betatron," *Med. Phys.* **1**, 62–67 (1974).

³L. B. Levy, R. G. Waggener, and A. E. Wright, "Measurement of primary bremsstrahlung spectrum from an 8-MeV linear accelerator," *Med. Phys.* **3**, 173–175 (1976).

⁴R. Nath and R. J. Schulz, "Determination of high-energy x-ray spectra by photoactivation," *Med. Phys.* **3**, 133–141 (1976).

⁵P. H. Huang, K. R. Kase, and B. E. Bjärngard, "Spectral characterization of 4 MV Bremsstrahlung by attenuation analysis," *Med. Phys.* **8**, 368–374 (1981).

⁶P. H. Huang, K. R. Kase, and B. E. Bjärngard, "Simulation studies of 4-MV x-ray spectral reconstruction by numerical analysis of transmission data," *Med. Phys.* **9**, 695–702 (1982).

⁷P. H. Huang, K. R. Kase, and B. E. Bjärngard, "Reconstruction of 4-MV bremsstrahlung spectra from measured transmission data," *Med. Phys.* **10**, 778–785 (1983).

⁸R. P. Lambert, J. W. Jury, and N. K. Sherman, "Measurement of bremsstrahlung spectra from 25 MeV electrons on Ta as a function of radiator thickness and emission angle," *Nucl. Instrum. Methods* **214**, 349–360 (1983).

⁹J. Brownridge, S. Samnick, P. Stiles, P. Tipton, J. Veselka, and N. Yeh, "Determination of the photon spectrum of a clinical accelerator," *Med. Phys.* **11**, 794–796 (1984).

¹⁰B. R. Archer, P. R. Almond, and L. K. Wagner, "Application of a Laplace transform pair model for high energy x-ray spectral reconstruction," *Med. Phys.* **12**, 630–633 (1985).

¹¹S. D. Ahuja, P. G. Steward, S. R. Tapankumar, and E. D. Slessinger,

"Estimated spectrum of a 4-MV therapeutic beam," *Med. Phys.* **13**, 368–373 (1986).

¹²A. Ahnesjo and P. Andreo, "Determination of effective bremsstrahlung spectra and electron contamination for photon dose calculations," *Phys. Med. Biol.* **34**, 1451–1464 (1989).

¹³C. R. Baker, Ph.D. thesis, University of Surrey, UK, 1993.

¹⁴M. Krmar, J. Slivka, I. Bikit, M. Veskovc, L. Conkic, M. Bistrovic, and A. Rudic, "A new method for the measurement of bremsstrahlung spectra," *Phys. Med. Biol.* **38**, 533–544 (1993).

¹⁵C. R. Baker, B. Ama'ee, and N. M. Spyrou, "Reconstruction of megavoltage photon spectra by attenuation analysis," *Phys. Med. Biol.* **40**, 529–542 (1995).

¹⁶C. R. Baker and K. K. Peck, "Reconstruction of 6 MV photon spectra from measured transmission including maximum energy estimation," *Phys. Med. Biol.* **42**, 2041–2051 (1997).

¹⁷A. Catala, P. Francois, J. Bonnet, and C. Scouamec, "Reconstruction of 12 MV bremsstrahlung spectra from measured transmission data by direct resolution of the numeric system $AF=T$," *Med. Phys.* **22**, 3–10 (1995).

¹⁸P. Francois, F. Coste, J. Bonnet, and O. Caselles, "Validation of reconstructed bremsstrahlung spectra between 6 MV and 25 MV from measured transmission data," *Med. Phys.* **24**, 769–773 (1997).

¹⁹A. Nisbet, H. Weatherburn, J. D. Fenwick, and G. McVey, "Spectral reconstruction of clinical megavoltage photon beams and the implications of spectral determination on the dosimetry of such beams," *Phys. Med. Biol.* **43**, 1507–1521 (1998).

²⁰R. Mohan, C. Chui, and L. Lidofsky, "Energy and angular distributions of photons from medical linear accelerators," *Med. Phys.* **12**, 592–597 (1985).

²¹D. W. O. Rogers, B. A. Faddegon, G. X. Ding, C. M. Ma, J. Wei, and T. R. Mackie, "BEAM: A Monte Carlo code to simulate radiotherapy treatment units," *Med. Phys.* **22**, 503–524 (1995).

²²J. A. Purdy, W. Harms, W. F. Hanson, P. Kennedy, T. Kirby, A. Niroomand-Rad, and J. R. Palta, AAPM RTC TG-46: X-ray Beam Central Axis Depth-Dose Data for Use in Radiation Therapy, *Med. Phys.* [1997 (draft approved by Radiation Therapy Committee)].

²³D. Sheikh-Bagheri, D. W. O. Rogers, C. K. Ross, and J. P. Seuntjens, "Comparison of measured and Monte Carlo calculated dose distributions from the NRC linac," *Med. Phys.* **27**, 2256–2266 (2000).

²⁴G. Mora, A. Maio, and D. W. O. Rogers, "Monte Carlo simulation of a typical ⁶⁰Co therapy source," *Med. Phys.* **26**, 2494–2502 (1999).

²⁵P. R. Almond, P. J. Biggs, B. M. Coursey, W. F. Hanson, M. S. Huq, R. Nath, and D. W. O. Rogers, "AAPM's TG-51 protocol for clinical reference dosimetry of high-energy photon and electron beams," *Med. Phys.* **26**, 1847–1870 (1999).

²⁶D. W. O. Rogers, Fundamentals of dosimetry based on absorbed-dose standards, in *Teletherapy Physics, Present and Future*, edited by J. R. Palta and T. R. Mackie (AAPM, Washington, DC, 1996), pp. 319–356.

²⁷B. A. Faddegon, P. O'Brien, and D. L. D. Mason, "The flatness of Siemens linear accelerator x-ray fields," *Med. Phys.* **26**, 220–228 (1999).

²⁸D. Sheikh-Bagheri, Ph.D. thesis, Carleton University, Ottawa, 1999.

²⁹R. Brun, O. Couet, C. Vandoni, and P. Zanarini, PAW User Guide, CERN Computer Center, Geneva, Switzerland, 1992.

³⁰J. R. Palta, K. Ayyangar, I. Daftari, and N. Suntharalingam, "Characteristics of photon beams from Philips SL25 linear accelerators," *Med. Phys.* **17**, 106–116 (1990).